THE JOURNAL OF PHYSICAL CHEMISTRY A

Article

pubs.acs.org/JPCA

Approximate Spin-Projected Density-Based Romberg Differentiation Procedure to Evaluate the Second-Hyperpolarizability of *p*-Quinodimethane and Twisted Ethylene and Their Diradical Character Dependence

Marc de Wergifosse*[,†,‡]

[†]Laboratory of Theoretical Chemistry, University of Namur, Rue de Bruxelles 61, 5000 Namur, Belgium

[‡]Department of Chemistry, University of Southern California, 90089-0482 Los Angeles, California, United States

Supporting Information

ABSTRACT: The evaluation of the static second hyperpolarizability (γ) of diradical species is a challenging task due to the use of spin-unrestricted methods, which may suffer from spin contamination. Here, we present the methodological aspect of a density-based differentiation procedure to evaluate static polarizability and hyperpolarizabilities. The finite-field calculations are done on the spin-projected electron density to remove the spin contamination, and the automatized Romberg's differentiation procedure is used to improve the numerical accuracy in the finite-field method. This implementation is tested in the present report for the challenging case of the evaluation of the second hyperpolarizability of the singlet ground state of *p*-quinodimethane (PQM) for the equilibrium geometry as well as for a stretched geometry where the diradical character of PQM is increased, and for twisted ethylene models where the diradical character changes with the dihedral angle. The application of the approximate spin-projected (ASP) scheme leads to a major improvement of the density functional theory calculations. In particular, for PQM models, BHandHLYP functional reproduces the UCCSD(T) values when the diradical character is below 0.5. The visualization of the γ-densities shows that (i) when increasing the diradical character, the amount of γ-density increases on the $-CH_2^{\bullet}$ extremities, and (ii) the ASP scheme decreases the amount of "p-like" γ-density for diradical character below 0.4, and increases it for larger diradical character. For twisted ethylene model, we show that the UCCSD(T) reference values can be reproduced by the ASP-UB3LYP method for $y < 0.4$ and by the ASP-UBHandHLYP method for $y > 0.6$. To best reproduce the UCCSD(T) reference calculations, the amount of exact exchange in hybrid functionals needs to be tuned along the range of diradical characters.

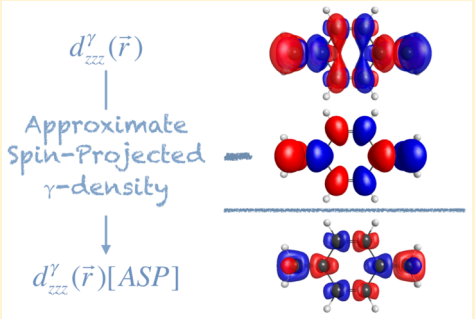

1. INTRODUCTION

The nonlinear optical (NLO) properties of matter are central to various technologies (including frequency multipliers, space communications, and NLO imaging microscopies).[1,2] Organic molecules are particularly promising in this respect due to their short response time as well as to the possibility to modify their structure−property relationship by synthesis of new derivatives.[3] A multidisciplinary approach is needed to design efficient organic NLO compounds. This includes their synthesis and experimental/theoretical characterizations. However, the theoretical prediction of the NLO properties of organic molecules remains a challenge due to the need to consider many subtle issues[4−6] such as accounting for electron correlation, vibrational contributions, effect of surroundings, and frequency dispersion. To address such issues, hierarchies of approximate methods and interpretation schemes have been developed.[2,7]

In 1989, Chopra et al.[8] introduced the idea that the NLO properties can be interpreted in terms of spatial regions that contribute to the field dependence of the electron density. The electron density is expanded in Taylor series as a function of the electric field components, in the same way as it is done for the energy or the dipole moment. Density derivatives are the parameters of the Taylor expansion of the electron density, and they can be obtained by the finite-field method. The dipole moment expansion can simply be recovered by integration of the position vector times the electron density. In the same way, (hyper)polarizabilities can be obtained by integration over their corresponding density derivatives. They also showed that it is possible to partition the density derivatives into contributions from individual orbitals or groups of orbitals. Following this, it has been applied in different contexts. In 1991, Nakano et al.[9] used for the first time the third derivative of the electron density (the γ-density) to resolve the spatial characteristics of the static second hyperpolarizability (γ) of substituted polydiacetylenes. In 1995, Champagne et al.[10] investigated the origin of the large difference in the static vibrational polarizability of polyethylene and polysilane (all-trans) by performing finite-deformation calculations and analyzed the

Received: February 28, 2016
Revised: April 9, 2016
Published: April 11, 2016

DOI: 10.1021/acs.jpca.6b02076
J. Phys. Chem. A 2016, 120, 2727−2736

induced electron density variations. In 1996, Nakano et al.[11] proposed a new method to analyze dynamic (hyper)-polarizabities in the presence of a time-dependent electric field, where they introduced the concept of "dynamic (hyper)polarizability density". This allows the visualization of dynamic electron fluctuation and relaxation processes. The same year, they investigated the shape of the γ-density of H_2NO and H_2CO.[12] They concluded that MP2 is able to reproduce the shape of the γ-density of H_2CO but not of H_2NO. In 2002, with the semiempirical INDO/S method, Nakano et al.[13] explored the relationship between γ and molecular architecture in phenylacetylene dendrimers using the γ-density analysis. In a large phenylacetylene dendrimer (24 units), they found that the spatial contributions to γ originate from the fractal architecture. In 2012, Yang and co-workers[14] proposed to decompose the first hyperpolarizability in local and nonlocal contributions by partitioning the electron density using the Hirshfeld partitioning analysis. This scheme has been applied to six prototypical donor−acceptor molecules for which the local and nonlocal hyperpolarizabilities are evaluated based on their MP2 densities. Recently, to predict the linear and second-order nonlinear susceptibilities of molecular crystals, Seidler et.al.[15] have considered the "quantum theory of atoms in molecules" to divide the electron density between submolecular "atoms" sites to distribute the polarizability tensors and to predict accurately local field tensors.

In 2011, Nakano et al.[16] have developed a method using the density derivatives to analyze the (hyper)polarizabilities of open-shell systems. They proposed to remove the spin-contamination inherent to the use of a spin-unrestricted method by using an approximate spin-projected (ASP) scheme based on the natural orbitals and the spin-projected occupation numbers.[17] When using broken symmetry schemes, it is essential to remove the spin contamination to obtain correct molecular structures[18] and magnetic properties.[19,20] In 2014, we proposed an automatization of the Romberg's scheme to improve the numerical accuracy in the finite-field (FF) method to evaluate molecular static hyperpolarizabilities.[21] Further, the same study showed that accurate numerical derivatives can be obtained using Romberg's method, where the Romberg's triangular table is analyzed considering the field amplitude error and the iteration error. The hyperpolarizability values so obtained have the same accuracy as those obtained analytically. Recently, we studied the γ of trimethylenemethane (TMM) and two 1,3-dipole derivatives (NXA and OXA) in their triplet ground state.[22] We used the coupled-cluster with the inclusion of singles and doubles as well as perturbative estimate of the triples (UCCSD(T)) method as reference. We showed that γ decreases from TMM to NXA and OXA, following the opposite order of their permanent dipole moments. Then, the UCCSD(T) results were used to assess wave function- and density functional theory (DFT)-based methods. We also removed the spin contamination from the DFT calculations by using the approximate spin-projection scheme proposed by Nakano and co-workers,[16] where the numerical differentiation was done on the spin-projected electron density using the automatized Romberg procedure[21] we developed. Since the spin contamination of the triplet state is negligible, this new method has a little impact.

In 2013, we were interested in the evaluation of the hyperpolarizabilities of three *p*-quinodimethane (PQM) derivatives with low diradical character.[23] In particular, the performance of DFT-based methods was assessed with respect to the CCSD(T) level of calculation. We concluded that these systems are not well treated by DFT method with the considered set of exchange-correlation (XC) functionals, where the results are spin-contaminated. Before that, in 2005, the dependence of γ on the diradical character (y) was investigated using several different wave function and DFT methods with a relatively small basis set (6-31G*+*p*) by Nakano et al.[24] To tune the diradical character of singlet diradical systems, the PQM molecule with different exocyclic carbon−carbon bond lengths was used. They found that PQM has a quinoid equilibrium geometry, whereas when stretching exocyclic C−C bonds, the diradical character increases. The main conclusion was that an intermediate diradical character enhanced the γ values for singlet diradical systems. They also found that their DFT calculations failed to reproduce the UCCSD(T) reference calculations. Following this, in 2010, Nakano et al.[25] applied the ASP scheme to PQM models with the same basis set. They concluded that the ASP LC-UBLYP (μ = 0.47) method reproduces semiqualitatively the diradical dependence of γ. They also provided a succinct analysis of the γ-density as a function of y. They stated that the shape of the γ-density is the same for all the range of y and that the dominant contribution to the response comes from the $-CH_2^{\bullet}$ extremities. The difference between the spin-projected and nonprojected γ-densities was also provided. They showed that the correction applied on all C atom γ-density contributions with alternating sign and that the sign of the correction is reversed between y = 0.257 and 0.491.

In the article about the PQM models in 2005, Nakano et al.[24] also provided a study about the γ of twisted ethylene geometries (from 55° to 90°) and showed the dependence of γ as a function of the diradical character at the UCCSD(T)/6-31G**+*sp* level of theory. This was previously studied for dihedral angles from 0° to 75°, in 1999, by Yamada et al.[26] at the UHF, UQCISD, and UCCSD(T) levels of theory. They observed that the rotation of the CH_2 group changes the γ-response significantly, and therefore the computed γ is considerably influenced by the level of treatment. Recently, Mondal et al.[27] characterized the γ of twisted ethylene geometries with MRCISD, CASSCF(4,4), and DFT methods. In particular, they used spin-projected UDFT method, without providing any information about the methodology they used. They obtained almost the same results with and without spin projection and concluded that the spin contamination is not the only parameter that influences the failure of DFT method to describe the γ of twisted ethylene models. Nevertheless, they stated that LC-UBLYP and UBHandHLYP results are similar to the MRCISD results.

In this article, the methodological aspects of the implementation of the density-based automatic Romberg differentiation procedure to evaluate the molecular static (hyper)polarizability are detailed in Section 2. In Section 3, this new implementation is tested for the evaluation of the second hyperpolarizability of (i) the PQM molecule in its singlet ground state as well as for PQM models, where the diradical character of PQM is increased when exocyclic C−C bonds are stretched, and (ii) twisted ethylene geometries where the diradical character is a function of the twisted angle. These particular applications are well-known cases where DFT γ-values fail to reproduce UCCSD(T) benchmarks for an open-shell system.[23−27] Thus, these are challenging cases to test our new implementation where we are able to remove the spin-contamination and thus correct the regular DFT values. In the

DOI: 10.1021/acs.jpca.6b02076
J. Phys. Chem. A 2016, 120, 2727−2736

first test case study, we use the 6-31G*+p basis set to compare the results obtained with the Romberg procedure to the ones obtained by Nakano et al.[25] We discuss their accuracy as well as the Romberg iteration error of our values. Following this, we compute the γ of PQM ground state and models characterized with the aug-cc-pVDZ basis set and compare to those obtained with the smaller basis set. Finally, the visualization of the hyperpolarizabity densities is used to understand the origin of the response in some more detail than in the previous analysis by Nakano et al.[25] In the second test case study, the ASP scheme is tested for a large set of different XC functionals. We also visualize the γ-densities for the most reliable functionals.

2. METHODOLOGY

2.1. Density-Based Automatized Romberg Differentiation Procedure. Applying light to matter results in a perturbation of the motion of electrons and nuclei owing to the electric field component of light. This can result in different phenomena such as absorption, emission, or scattering of the light. In all these processes, the motion of the electrons and nuclei is perturbed by the external electric field, and this interaction can be characterized by the variations of the molecular dipole moment under the form of a Taylor expansion:

$$\vec{\mu}(\vec{F}) = \vec{\mu}_0 + \vec{\alpha}\cdot\vec{F} + \frac{1}{2!}\overleftrightarrow{\beta} : \vec{F}\vec{F} + \frac{1}{3!}\overleftrightarrow{\gamma} \vdots \vec{F}\vec{F}\vec{F} + \ldots \tag{1}$$

The first term in the expansion, $\vec{\mu}_0$, is the intrinsic dipole moment vector, the second term $\vec{\alpha}$ is the polarizability tensor, and the higher-order terms are the nonlinear ones where $\overleftrightarrow{\beta}$ and $\overleftrightarrow{\gamma}$ are, respectively, the first and second hyperpolarizability tensors. The Taylor expansion is sometimes replaced by a power series, of which the consequence is to implicitly include the numerical $1/n!$ factor into the hyperpolarizabilities. These definitions correspond to different conventions, denoted T when using the Taylor expansion and B for the power series expansion.

The electronic dipole moment can also be obtained by integrating the position vector times the electron density as follows

$$\vec{\mu}(\vec{F}) = -\int \vec{r}\, d(\vec{r}, \vec{F})\mathrm{d}\vec{r} \tag{2}$$

where the electronic density is expressed as a Taylor expansion with respect to the external electric field:[5]

$$d(\vec{r}, \vec{F}) = d_0(\vec{r}) + \vec{d}_\alpha(\vec{r})\cdot\vec{F} + \frac{1}{2!}\vec{d}_\beta(\vec{r}) : \vec{F}\vec{F} + \frac{1}{3!}\overleftrightarrow{d}_\gamma(\vec{r}) \vdots \vec{F}\vec{F}\vec{F} + \ldots \tag{3}$$

Then, the electronic dipole moment is rewritten as

$$\vec{\mu}(\vec{F}) = -\int \vec{r}\left[d_0(\vec{r}) + \vec{d}_\alpha(\vec{r})\cdot\vec{F} + \frac{1}{2!}\vec{d}_\beta(\vec{r}) : \vec{F}\vec{F} + \frac{1}{3!}\overleftrightarrow{d}_\gamma(\vec{r}) \vdots \vec{F}\vec{F}\vec{F} + \ldots \right]\mathrm{d}\vec{r} \tag{4}$$

The polarizability, and the first and second hyperpolarizabilies, are defined as the integration of the position vector all over their respective densities:

$$\vec{\alpha} = -\int \vec{r}\vec{d}_\alpha(\vec{r})\mathrm{d}\vec{r} \tag{5}$$

$$\overleftrightarrow{\beta} = -\int \vec{r}\overleftrightarrow{d}_\beta(\vec{r})\mathrm{d}\vec{r} \tag{6}$$

$$\overleftrightarrow{\gamma} = -\int \vec{r}\overleftrightarrow{d}_\gamma(\vec{r})\mathrm{d}\vec{r} \tag{7}$$

In this context, if we consider a geometric progression of external electric fields $F(k) = a^k F_0$ for $k = 0, 1, \ldots$ where F_0 is the smallest field amplitude and a is the common ratio, the differentiation procedure can consist in combining electron density grids obtained for this series of electric field amplitudes. The finite difference expressions for the (hyper)polarized density tensor components read:

$$d_i^\alpha(\vec{r}, k) = \frac{d(\vec{r}, F_i(k)) - d(\vec{r}, F_{-i}(k))}{2a^k F_0} \tag{8}$$

$$d_{ii}^\beta(\vec{r}, k) = \frac{[d(\vec{r}, F_i(k)) + d(\vec{r}, F_{-i}(k))] - 2d(\vec{r}, 0)}{(a^k F_0)^2} \tag{9}$$

$$\begin{aligned} d_{ij}^\beta(\vec{r}, k) = \{&[d(\vec{r}, F_i(k)) + d(\vec{r}, F_{-i}(k))] \\ &+ [d(\vec{r}, F_j(k)) + d(\vec{r}, F_{-j}(k))] \\ &- [d(\vec{r}, F_{ij}(k)) + d(\vec{r}, F_{-i-j}(k))] \\ &- 2d(\vec{r}, 0)\}/\{2(a^k F_0)^2\} \end{aligned} \tag{10}$$

$$\begin{aligned} d_{iii}^\gamma(\vec{r}, k) = 3\{&[d(\vec{r}, F_i(k+1)) - d(\vec{r}, F_{-i}(k+1))] \\ &- a[d(\vec{r}, F_i(k)) - d(\vec{r}, F_{-i}(k))]\} \\ &/\{a(a^2 - 1)(a^k F_0)^3\} \end{aligned} \tag{11}$$

$$\begin{aligned} d_{ijj}^\gamma(\vec{r}, k) = \{&[d(\vec{r}, F_{ij}(k)) - d(\vec{r}, F_{-i-j}(k))] \\ &+ [d(\vec{r}, F_{i-j}(k)) - d(\vec{r}, F_{-ij}(k))] \\ &- 2[d(\vec{r}, F_i(k)) - d(\vec{r}, F_{-i}(k))]\}/\{2(a^k F_0)^3\} \end{aligned} \tag{12}$$

where the $\pm i$ and $\pm j$ field indices refer to the field directions. The static (hyper)polarizability tensor components corresponding to the zero-order iteration is obtained by the following integrations:

$$\alpha_{mi}(k, 0) = -\int_{\text{grid}} r_m d_i^\alpha(\vec{r}, k)\mathrm{d}\vec{r} \tag{13}$$

$$\beta_{mij}(k, 0) = -\int_{\text{grid}} r_m d_{ij}^\beta(\vec{r}, k)\mathrm{d}\vec{r} \tag{14}$$

$$\gamma_{mijl}(k, 0) = -\int_{\text{grid}} r_m d_{ijl}^\gamma(\vec{r}, k)\mathrm{d}\vec{r} \tag{15}$$

where the m field index refers to a field direction, that is, x, y, or z. The Romberg recursive expression is used to remove the contaminations from higher-order hyperpolarizabilities:

$$\xi(k, n) = \frac{a^{2n}\xi(k, n-1) - \xi(k+1, n-1)}{a^{2n} - 1} \tag{16}$$

Romberg iterations can be represented in a triangular table that allows visualizing the convergence of the numerical derivative.

DOI: 10.1021/acs.jpca.6b02076
J. Phys. Chem. A 2016, 120, 2727−2736

An example of Romberg triangular table is provided in Table 1 for the determination of the γ_{zzzz} of PQM-2 (see below) at the

Table 1. Romberg Triangular Table[a] for the Determination of the γ_{zzzz} of PQM-2 at the ASP-BHandHLYP/aug-cc-pVDZ Level with a Step-Size of 2.0 and a Smallest Field Amplitude of 0.0004 a.u.

	n=0		n=1		n=2		n=3
k=0	265802.9	6.5	265809.4	3.9	265813.3	1.0	265814.3
	-19.6		-58.6		-60.8		
k=1	265783.2	-32.4	265750.8	1.7	**265752.5**		
	97.3		-25.8				
k=2	265880.5	-155.4	265725.0				
	466.3						
k=3	266346.8						

[a]The field amplitude errors and the iteration order errors are written in blue and in red, respectively. The final field amplitude and iteration errors are underlined and in bold. The final γ_{zzzz} is in bold. The stable sub-triangle is in gray.

ASP-BHandHLYP/aug-cc-pVDZ level with a step-size of 2.0 and a smallest field amplitude of 0.0004 au. The systematic analysis of this table is performed by an automatized procedure we have proposed in 2014.[21] Indeed, for any molecular systems there exists a set of field amplitudes defined by upper and lower bounds where we have a stable finite differentiation. The lower bound is defined by a large rounding error related to the energy convergence threshold and the density grid accuracy. The largest value of this set of fields depends of the particular field amplitude where the ground state intersects with the excited states. This set of "stable" field amplitudes defines a sub-triangular table (see the gray area in Table 1). To determine the subset of field amplitudes, the automatic procedure analyzes the field amplitude errors:

$$\varepsilon_k(n) = \xi(k+1, n) - \xi(k, n) \tag{17}$$

Since the field amplitude error satisfies the Romberg recursive expression, the field errors should decrease along the Romberg iterations. Moreover, the iteration error probes the convergence between successive Romberg iterations:

$$\varepsilon_n(k) = \xi(k, n+1) - \xi(k, n) \tag{18}$$

The automatic analysis of these quantities leads to a converged value $\xi(k,n+1)$ with a final iteration error $\varepsilon_n(k)$.[21] Note that if the field window has not been wisely chosen at the beginning, the automatic procedure will fail to locate a stable sub-triangular table. Nevertheless, the final iteration error will always provide reliable information about the stability of this procedure.

It is also possible to obtain a converged (hyper)polarized density by using the "Romberg procedure". Indeed, if the automatic Romberg differentiation procedure has selected a converged value $\xi(k,n)$, the corresponding converged density is obtained by the following recursive expression:

$$d^{\xi}(\vec{r}, k, n) = \frac{a^{2n} d^{\xi}(\vec{r}, k, n-1) - d^{\xi}(\vec{r}, k+1, n-1)}{a^{2n} - 1} \tag{19}$$

The integration of the position vector times this density will give back the same $\xi(k,n)$ value. This converged (hyper)-polarized density gives a visual insight into the origin of the response.

2.2. Approximated Spin-Projected Density Scheme.

To remove the spin contamination in open-shell calculations, spin-projected densities can be used.[16] To our knowledge, this is the only way to remove the spin contamination to determine (hyper)polarizabilities at the DFT level of calculation. The spin-projected occupation numbers are used to correct the electron density and are defined as

$$n^{\mathrm{SP}}_{\mathrm{HONO}-i} = \frac{(n_{\mathrm{HONO}-i})^2}{1 + \left(\frac{n_{\mathrm{HONO}-i} - n_{\mathrm{LUNO}+i}}{2}\right)^2}$$

$$n^{\mathrm{SP}}_{\mathrm{LUNO}+i} = \frac{(n_{\mathrm{LUNO}+i})^2}{1 + \left(\frac{n_{\mathrm{HONO}-i} - n_{\mathrm{LUNO}+i}}{2}\right)^2} \tag{20}$$

The approximate spin-projected one-electron density $d^{\mathrm{SP}}(\vec{r})$ reads:

$$d^{\mathrm{SP}}(\vec{r}) = \sum_{i=0}^{N/2-1} [n^{\mathrm{SP}}_{\mathrm{HONO}-i} \phi^{*}_{\mathrm{HONO}-i}(\vec{r}) \phi_{\mathrm{HONO}-i}(\vec{r}) + n^{\mathrm{SP}}_{\mathrm{LUNO}+i} \phi^{*}_{\mathrm{LUNO}+i}(\vec{r}) \phi_{\mathrm{LUNO}+i}(\vec{r})] \tag{21}$$

This scheme is approximated since the natural orbitals are not spin-projected, only the occupation numbers are. In this way, the spin-projected (hyper)polarizability can be determined accurately by using the automatic Romberg differentiation procedure.[21]

2.3. Computational Details.

The PQM diradical is used in the present work as the first illustrative case study where the diagonal (longitudinal) γ_{zzzz} component is determined by the ASP method with different DFT XC functionals. We consider the γ_{zzzz} component, since it has the largest response. Figure 1

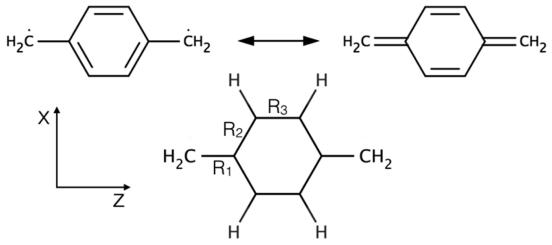

Figure 1. Resonance structure and key geometrical parameters of PQM considering a D_{2h} symmetry.

presents the two resonance forms of PQM diradical as well as its three key geometrical parameters. The singlet ground-state geometry of PQM as well as its UCCSD(T)/aug-cc-pVDZ γ_{zzzz} reference value of 150×10^3 a.u. were taken from ref 23. To estimate the influence of the diradical character over the second hyperpolarizability, we followed the same methodology as Nakano et al.[24,25] To increase the diradical nature of PQM, they have considered several PQM models of D_{2h} symmetry with bond length R_1 changing from 1.350 to1.700 Å under the constraint of $R_2 = R_3 = 1.400$ Å. The geometrical parameters of seven PQM geometries (including the stable singlet ground state) are presented in Table 2 as well as their respective diradical character (y) obtained at the UHF/aug-cc-pVDZ level of theory. The diradical character is defined as

$$y = 1 - \frac{2T}{1 + T^2} \tag{22}$$

DOI: 10.1021/acs.jpca.6b02076
J. Phys. Chem. A 2016, 120, 2727−2736

Table 2. Diradical Charaters and Geometrical Parameters[a] of PQM Models

name	y	R_1 (Å)	R_2 (Å)	R_3 (Å)
PQM-1	0.134	1.351	1.460	1.346
PQM-2	0.244	1.350	1.400	1.400
PQM-3	0.323	1.400	1.400	1.400
PQM-4	0.404	1.450	1.400	1.400
PQM-5	0.482	1.500	1.400	1.400
PQM-6	0.555	1.550	1.400	1.400
PQM-7	0.621	1.600	1.400	1.400
PQM-8	0.729	1.700	1.400	1.400

[a]PQM-1 is the equilibrium geometry. The diradical character was computed at UHF/aug-cc-pVDZ level of theory.

where $T = \frac{n_{HONO} - n_{LUNO}}{2}$, and n is the occupation number of the natural orbitals.[24] As explained in ref 24, they state "These boldly approximate models are expected to mimic the change in diradical character of real systems since the variation in R_1 mainly corresponds to the dissociation of π bonds. Although these models lack the concomitant recovery of aromaticity of the central benzene ring present in real systems (...)". Following the recommendations of our previous study on PQM, the aug-cc-pVDZ basis set was employed for all the calculations,[23] except for the comparison to the previous results of Nakano et al.[25] obtained with the 6-31G*+p basis set.

In the second illustrative case study, we consider the same twisted ethylene models as in ref 24. We used a C=C bond length of 1.3376 Å, C−H of 1.0868 Å, and an H−C−H angle of 121.58°. Those parameters come from the optimization of the planar ethylene at the QCISD/6-311G** level of theory. We vary the twisted angle between the two H−C−H planes from 55° to 85° with step size of 5°. In Table 3, the diradical

Table 3. Diradical Charater[a] and Twisted Angle of Ethylene Models

name	y	θ (deg)
ETH-1	0.102	55
ETH-2	0.157	60
ETH-3	0.234	65
ETH-4	0.337	70
ETH-5	0.467	75
ETH-6	0.626	80
ETH-7	0.807	85

[a]The diradical character was computed at UHF/aug-cc-pVDZ level of theory.

character determined at the UHF/aug-cc-pVDZ level of theory is provided. We used the aug-cc-pVTZ basis set to evaluate the longitudinal γ_{zzzz} component with the ASP method.

The UCCSD(T) was used as reference method to assess the performance of several XC functionals in unrestricted DFT computations. In particular, the role of the HF exchange (HF exc) in the XC functional is assessed with this set of functionals: BLYP (0% HF exc), B3LYP (20% HF exc), BHandHLYP (50% HF exc), LC-BLYP (μ = 0.33 and μ = 0.47, default in Gaussian09[28]) including 100% of HF exc at large interelectronic distances, M06 (0% HF exc), and M06-2X (54% HF exc) functionals. In the case of LC-BLYP, Bonness et al.[29] have shown that the LC-UBLYP method with μ = 0.3−0.5 is adequate for calculating γ of π-conjugated diradical systems.

To reproduce UCCSD(T) values, the approximated spin projected DFT γ_{zzzz} values were determined by the spin-projected density-based automatized Romberg differentiation procedure described above. However, the DFT and UCCSD-(T) γ_{zzzz} values were calculated using the energy-based automatic Romberg differentiation procedure.[21] In the energy-based and density-based FF calculations, we used: $\pm 2^k \times 0.0004$ or $\pm \sqrt{2}^k \times 0.0004$ or $\pm \sqrt{2}^k \times 0.0008$ with k going from 0 to 5 or 10, as geometric progression of external electric field amplitudes. We used energy convergence thresholds from 1×10^{-9} to 1×10^{-11} a.u. All the calculations used unrestricted methods. The precision of the density-based computations depends on the grid parameters and on the accuracy of the numerical integration. Small tests were performed on the integration of the electron density of the H_2 molecules with different box sizes and with different integration methods (Table S1). From those tests, it appears that the simple cuboid integration is more accurate, for the same grid size, than other methods based on the Newton−Cotes rules. In that case, the integration interval is enlarged since more points are needed to evaluate it. In Table S1, it is shown that with the diminution of the grid size, the accuracy of the number of electrons is decreasing, but the density size is also smaller. Since memory disc requirement is the principal bottleneck of this method (each density calculation takes ∼35 mb of disc space for PQM), we chose a cube mesh generated every 0.1 Å in a rectangular box with ±4 Å of vacuum around the molecule.

We used the Gaussian09 package[28] for the computations. The automatic Romberg differentiations were performed using the T-REX program.[21] The T convention was used for the definition of the second hyperpolarizability.

3. RESULTS AND DISCUSSION

3.1. *p*-Quinodimethane. In ref 25, Nakano et al. tested the ASP scheme on the PQM models for a set of XC functionals. Using the 6-31G*+p basis set, they showed that ASP-LC-UBLYP (μ = 0.47) functional can reproduce semiquantitatively the UCCSD(T) reference values. Their values were converged to a numerical accuracy of less than 1% using a simple multiple point FF formula. We recomputed those values using our new implementation that utilizes the Romberg procedure, as well as the ASP-UBHandHLYP γ_{zzzz} values. In Figure 2, the percentage

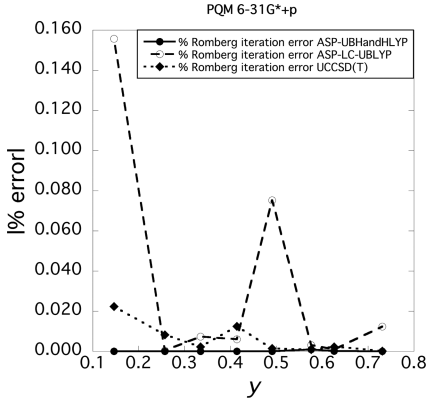

Figure 2. Romberg iteration error for the determination of the second hyperpolarizability as a function of the diradical character for the PQM models obtained at the ASP-UBHandHLYP, ASP-LC-UBLYP, and UCCSD(T) levels of theory with the 6-31G*+p basis set. Lines are used to connect the points to improve readability.

DOI: 10.1021/acs.jpca.6b02076
J. Phys. Chem. A 2016, 120, 2727−2736

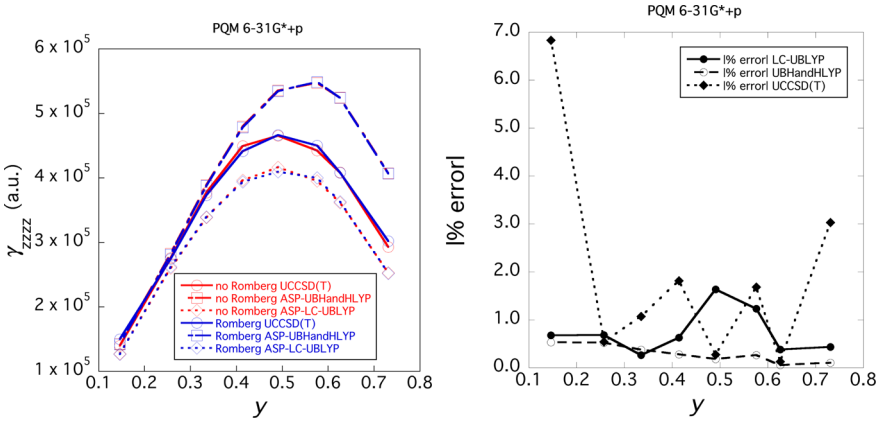

Figure 3. Comparison between the second hyperpolarizability obtained with and without the Romberg procedure as a function of the diradical character for the PQM models obtained at the ASP-UBHandHLYP, ASP-LC-UBLYP, and UCCSD(T) levels of theory with the 6-31G*+*p* basis set. The second graph provides the percentage of error with respect to Romberg values as a function of the diradical character. Lines are used to connect the points to improve readability. The results without Romberg procedure were taken from ref 25 (courtesy of Prof. M. Nakano).

of Romberg iteration error is presented for those two functionals as well as for the UCCSD(T) method, where the differentiation is based on the energy. The maximum iteration error is obtained for the PQM-1 at the ASP-LC-UBLYP level, with a value of 0.156%. Note that this error can be easily reduced by decreasing the step size of the geometrical progression of fields (here we use a step size of 2.0) as well as by using a finer grid. For ASP-UBHandHLYP, we have a maximum iteration error of 9.50×10^{-4}, using the same field amplitudes. In Figure 3, we compare the results of Nakano et al.[25] to the values we computed. We also provide the percentage of error with respect to our values as a function of the diradical character. First, their ASP-UBHandHLYP are very well converged, with less than 0.532% of error. This is because the derivative is relatively stable for a large range of field amplitudes as indicated by the Romberg iteration error in Figure 2. Second, for ASP-LC-UBLYP functional, we note that the Romberg iteration error is relatively "large" for $y = 0.491$. Here the stable field window is narrower than for ASP-UBHandHLYP. Thus, using a simple multiple-point FF formula needs to be done carefully in that case. Their value has 1.63% of error with respect to ours. Still, this error value is quite low. Third, we have 6.83% of error for the UCCSD(T) value for the equilibrium geometry (PQM-1). But this can be because we used the geometry from ref 23 and not the same as them. Nevertheless, the errors are larger for the energy-based UCCSD(T) calculations. Note that we pay particular attention to the convergence threshold for the CCSD(T) calculation (1×10^{-11} Ha).

With the larger aug-cc-pVDZ basis set, the ratios between the DFT γ_{zzzz} values and the reference UCCSD(T) value for the singlet ground-state geometry of PQM (PQM-1) are presented in Figure 4. This also includes ratio with the ASP DFT γ_{zzzz} values. As we already found in ref 23, since the diradical character is small for PQM, not all XC functionals lead to unrestricted solutions. In fact, for PQM, only BHandHLYP, LC-BLYP with $\mu = 0.47$ give unrestricted solutions. The XC functionals with restricted solution predict too small values. This includes BLYP, B3LYP, LC-BLYP ($\mu = 0.33$), and M06-2X functionals all of which underestimate the reference by ~50%. However, M06 performs even worse and consistently underestimates γ_{zzzz} by 70%. BHandHLYP and LC-BLYP with $\mu = 0.47$ functionals overestimate the reference value by ~100%

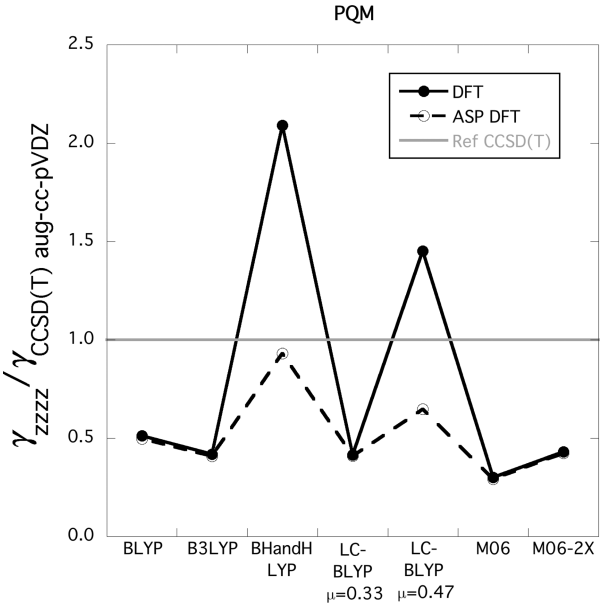

Figure 4. Electron correlation effects of DFT XC functionals on the second hyperpolarizability of PQM. Lines are used to connect the points to improve readability. This figure compares regular DFT values obtained with and without the approximate spin-projection scheme with respect to the UCCSD(T)/aug-cc-pVDZ γ_{zzzz} reference value.

and 50%, respectively. For those two functionals, the application of the ASP DFT scheme leads to a major improvement. For the BHandHLYP functional, the reference value is only underestimated by 7.0%. The LC-BLYP value, however, is 35% under the reference value. Note that the LC-BLYP ($\mu = 0.33$) functional gives a restricted solution, which is not the case with a range-separated parameter of 0.47.

Using the PQM models, the diradical character dependence of γ_{zzzz} is presented in Figure 5 for the two XC functionals with unrestricted solutions, in the case of PQM-1. Without the ASP scheme, as for the smaller basis set,[25] the two functionals are unable to reproduce the UCCSD(T) reference shape. However, when using the ASP scheme, the reference shape is qualitatively well reproduced by both functionals over the whole range of y values. This was already noted by Nakano et al.[25] However, with this larger basis set, their conclusion that

DOI: 10.1021/acs.jpca.6b02076
J. Phys. Chem. A 2016, 120, 2727−2736

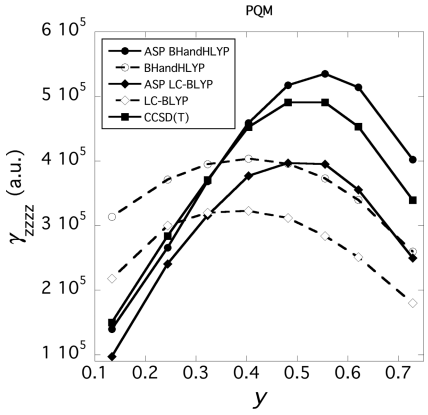

Figure 5. Diradical character dependence of γ_{zzzz} for the PQM models with BHandHLYP and LC-BLYP XC functionals. Lines are used to connect the points to improve readability. This figure compares regular DFT values obtained with and without the approximate spin-projection scheme to the UCCSD(T)/aug-cc-pVDZ γ_{zzzz} reference value.

ASP-LC-UBLYP method reproduces semiquantitatively the reference curve does not stand anymore since the discrepancy between the two curves is larger. Indeed, only the BHandHLYP functional is able to reproduce the UCCSD(T) γ_{zzzz} values, at least for diradical characters below ~0.500. In that threshold, the reference values are underestimated for PQM-1 and PQM-2 by 7.0% and 6.3%, respectively, and overestimated by 5.4% for PQM-5. This last percentage corresponds to a larger discrepancy since the absolute γ_{zzzz} value is larger than for the PQM model with smaller R_1 bond lengths. The best agreement is obtained for PQM-3 and PQM-4 with only 0.6% and 1.4% of difference with respect to the UCCSD(T) reference, respectively. Above a diradical character of 0.500, an overestimation of 9.0%, 13.4%, and 26.5% are obtained for PQM-6, PQM-7, and PQM-8, respectively. Since the spin-projection is only done on the occupation numbers and not on the natural orbitals, this method has difficulties to correct the second hyperpolarizability behavior for large diradical characters, but at least, it can provide an agreement with less than 10% of

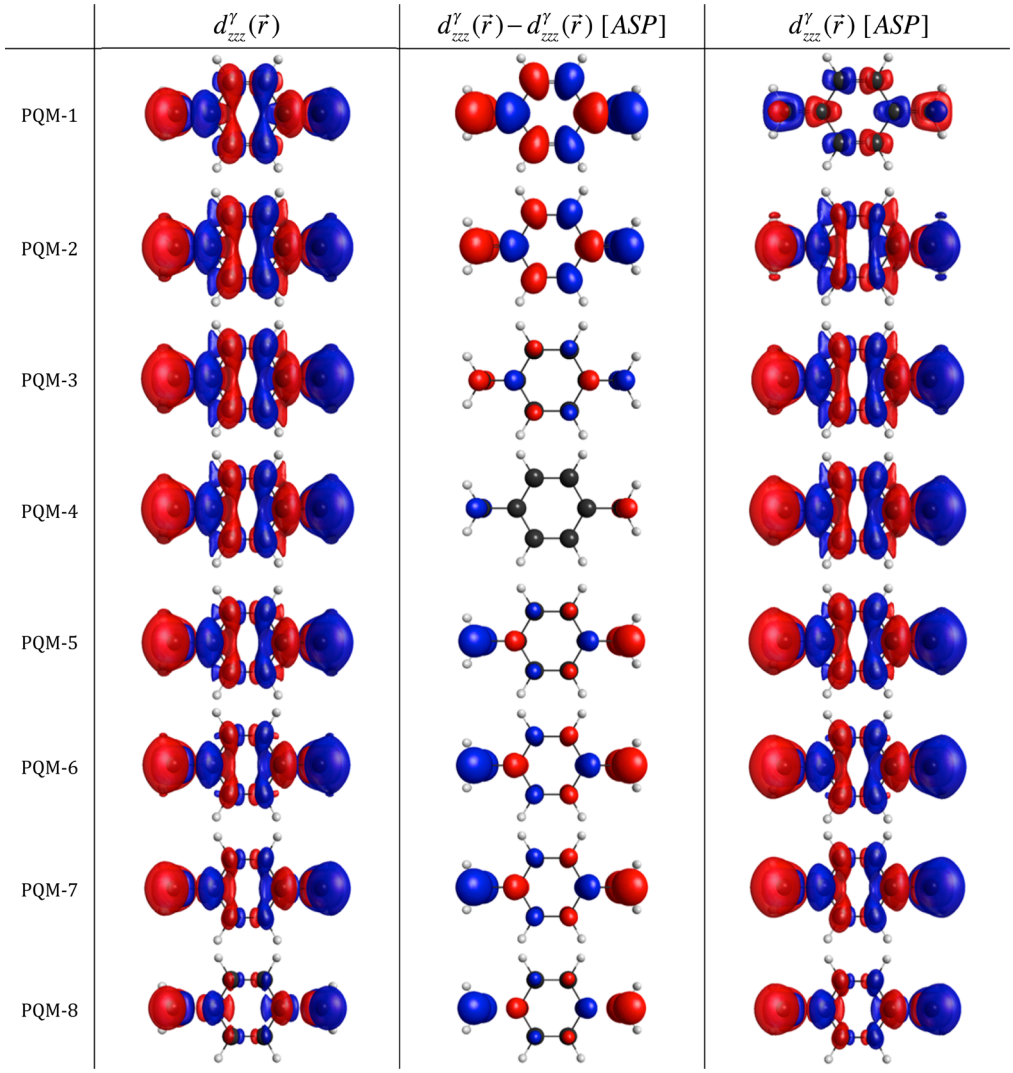

Figure 6. γ-densities (isovalue of 200 au) and the approximate spin-projected γ-densities are presented in columns 1 and 3, respectively. The differences between those two densities are presented in the second column. These γ-densities were used to obtain the diagonal γ_{zzzz} components as determined at the UBHandHLYP/aug-cc-pVDZ level of calculation with and without spin-projection. The blue/red colors show positive/negative densities.

DOI: 10.1021/acs.jpca.6b02076
J. Phys. Chem. A 2016, 120, 2727−2736

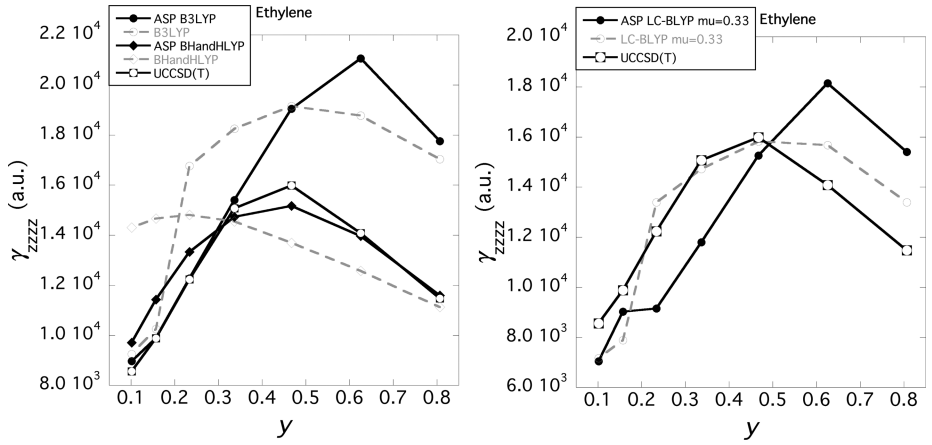

Figure 7. Diradical character dependence of γ_{zzzz} for the ethylene models with B3LYP, BHandHLYP, and LC-BLYP (μ = 0.33) XC functionals. Lines are used to connect the points to improve readability. These figures compare regular DFT values obtained with and without the approximate spin-projection scheme to the UCCSD(T)/aug-cc-pVTZ γ_{zzzz} reference value.

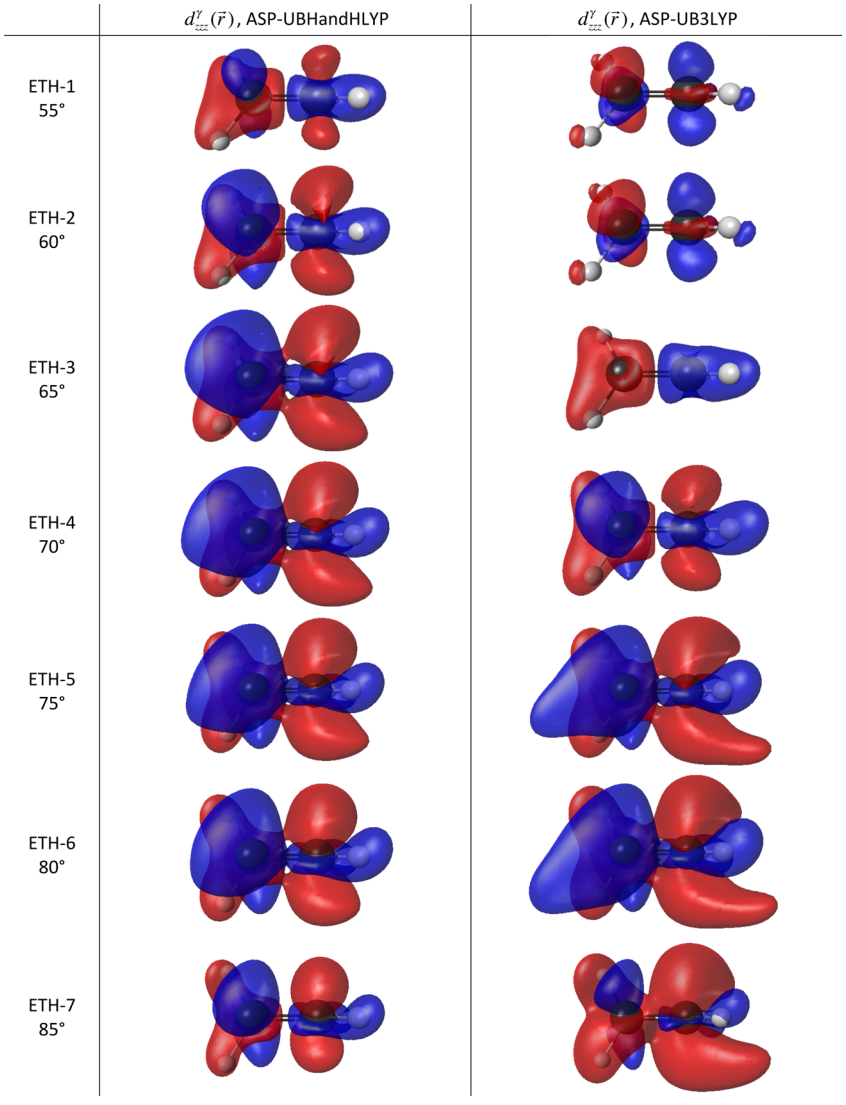

Figure 8. γ-densities (isovalue of 15 au) used to obtain the diagonal γ_{zzzz} components as determined at the ASP-UB3LYP/aug-cc-pVDZ and ASP-UBHandHLYP/aug-cc-pVDZ levels of calculation. The blue/red colors show positive/negative densities.

difference with respect to the reference for diradical character below 0.600.

In Figure 6, the UBHandHLYP/aug-cc-pVDZ γ-densities with and without approximated spin-projection employed to

DOI: 10.1021/acs.jpca.6b02076
J. Phys. Chem. A 2016, 120, 2727−2736

obtain the dominant diagonal γ_{zzzz} components for all the PQM models are presented for the same isovalue of 200 au We also presented the difference between these two densities $(d^{\gamma}_{zzz}(\vec{r}) - d^{\gamma}_{zzz}(\vec{r})[\mathrm{ASP}])$ to provide a visual representation of the impact of the ASP scheme on the γ-densities. By using the Romberg procedure, these γ-densities are converged. Note that Nakano et al.[25] have also provided the ASP-LC-UBLYP surfaces but only for three diradical characters. As already mention in the Introduction, they stated that the shape of the γ-density is the same for all the range of y and that the dominant contribution to the response comes from the $-CH_2^{\bullet}$ extremities. A quick look to our surfaces shows that, in fact, the PQM-1 γ-density is quite different from the others. Indeed, for PQM-1 (the singlet ground-state geometry), from the inspection of its key geometrical parameters, it is more quinoidic than aromatic. Consequently, with ASP scheme, the amount of density is more concentrated on double-bonds (R_1 and R_3) with a density node in the middle of the bond. The highest density is on the $-CH_2^{\bullet}$ extremities as already noted by Nakano et al.[25] The ASP scheme has strongly corrected the $d^{\gamma}_{zzz}(\vec{r})$ by removing a large amount of "p-like" γ-density on each carbon, in particular, on the $-CH_2^{\bullet}$ extremities. Going from PQM-1 to PQM-2, the main difference is that the geometrical parameters were chosen to have a pure aromatic geometry with $R_2 = R_3$. This increases the diradical character as well as the γ_{zzzz} response. The shape of the ASP $d^{\gamma}_{zzz}(\vec{r})$ changes drastically with a more complex arrangement, including the PQM-1 shape plus "p-like" contributions. First, there is now a contribution on the R_2 bond, and second, the amount of density has largely increased on $-CH_2^{\bullet}$ extremities leading to a larger γ_{zzzz} response. The ASP scheme provides the same type of corrections on the γ-density than for PQM-1 by removing contributions on each carbon but with a smaller impact. For larger R_1 bond lengths, An increase of the amount of $d^{\gamma}_{zzz}(\vec{r})$ on the $-CH_2^{\bullet}$ extremities is observed with the increase of the diradical character, which saturates when $y > 0.6$. Note that the ASP scheme decreases the γ-density for $y < 0.4$, and increases it with diradical characters above 0.4.

3.2. Twisted Ethylene. In Figure S1, using the twisted ethylene geometries, we present the diradical character dependence of γ_{zzzz} for all the XC correlation functionals (with and without ASP) considered in this study as well as for the UCCSD(T) reference. In Figure 7, we report only the UB3LYP, UBHandHLYP, and LC-UBLYP ($\mu = 0.33$) results. From all this set of XC functionals, only LC-UBLYP ($\mu = 0.33$) is able to reproduce the UCCSD(T) values without spin-projection, at least for y values of 0.336 and 0.467, with an underestimation of just 2.3% and 1.0%, respectively. For the ASP scheme, for a y-value below 0.4, ASP-UB3LYP reproduce the UCCSD(T) reference values with less than 4.7% of difference. The ASP-UBHandHLYP functional best reproduces the global UCCSD(T) shape and, in particular, for large y values of 0.626 and 0.807. The ASP-DFT γ_{zzzz} of the twisted ethylene models is really sensitive to the amount of exact exchange present in the functional. This is further confirmed by the visualization of the γ-density for both functionals (Figure 8), where the shape is really sensitive to the functional employed. For dihedral angles of 55° and 60°, the ASP-UB3LYP γ-density is dominated by "p-like" density on the two carbons. This is no more the case for a dihedral angle of 60°, where the density is dominated by "σ-like" density. Increasing the dihedral angle leads to the return of a "p-like" density on the two carbons. ASP-BHandHLYP method is not able to describe this change of γ-density shape. While ASP-BHandHLYP reproduces well the change of "p-like" γ-density for $y > 0.4$, this is not the case for ASP-UB3LYP. The amount of exact exchange in the functional must be tuned along the range of diradical characters considered to best reproduce the UCCSD(T) reference. Note that the ASP scheme changes the DFT results drastically, unlike the case reported by Mondal et al.[27]

4. CONCLUSIONS

In this article, we have presented the methodological aspects of the implementation of the density-based automatic Romberg differentiation procedure to evaluate molecular static (hyper)-polarizabilities. The use of this method has been motivated by the fact that spin contamination can be removed from broken-symmetry calculations. We assess the performance of this method by applying it to two well-known cases where the DFT method is impacted by spin contamination and fails to reproduce UCCSD(T) static second hyperpolarizabilities of the singlet ground state of PQM as well as PQM models with higher diradical character, and twisted ethylene models. For the singlet ground state of PQM, we have shown that the application of the ASP scheme leads to a major improvement of the DFT calculations, where the BHandHLYP functional underestimates by only 7% the UCCSD(T) value. The application of the ASP scheme at the DFT level on PQM models allows to reproduce qualitatively the evolution of the UCCSD(T) γ as a function of the diradical character. In particular, the BHandHLYP functional is able to reproduce the UCCSD(T) values for diradical character below 0.5. Moreover, the visualization of the γ-densities shows that (i) with an increase of the diradical character, the amount of γ-density increases on the $-CH_2^{\bullet}$ extremities, and (ii) the ASP scheme decreases the amount of "p-like" γ-density for diradical character below 0.4 and increases it for larger diradical character. In case of the twisted ethylene models, we have shown that ASP-UB3LYP method is able to reproduce the UCCSD(T) reference values for $y < 0.4$ and ASP-UBHandHLYP method for $y > 0.6$. To best reproduce the UCCSD(T) reference calculations, the amount of exact exchange in hybrid functionals must be tuned along the range of diradical characters. We also find that the ASP scheme is really important to remove the spin-contamination in these systems.

■ ASSOCIATED CONTENT

Supporting Information

The Supporting Information is available free of charge on the ACS Publications website at DOI: 10.1021/acs.jpca.6b02076.

Box sizes and integration methods tests on the integration of the M06-2X/aug-cc-pvdz electron density of the H_2 molecule (d_{H-H} = 0.74 Å). Diradical character dependence of γ_{zzzz} for the ethylene models with all the XC functionals considered with and without the approximate spin-projection scheme with respect to the UCCSD(T)/aug-cc-pVTZ γ_{zzzz} reference value. (PDF)

■ AUTHOR INFORMATION

Corresponding Author

*E-mail: marc.dewergifosse@unamur.be. Phone: +32 (0)81 724 547.

DOI: 10.1021/acs.jpca.6b02076
J. Phys. Chem. A 2016, 120, 2727−2736

Notes

The authors declare no competing financial interest.

■ ACKNOWLEDGMENTS

The author is grateful to Profs. B. Champagne and M. Nakano for their insightful remarks and helpful suggestions. In particular, I am deeply grateful to Prof. Nakano to provide me his data about PQM. I would like also to thank Drs. S. Gozem and K. Nanda for their useful feedback regarding the manuscript. The calculations were performed on the computers of the Consortium des Équipements de Calcul Intensif and mostly those of the Technological Platform of High-Performance Computing, for which we gratefully acknowledge the financial support of the FNRS-FRFC (Conventions No. 2.4.617.07.F and 2.5020.11) and of the Univ. of Namur.

■ REFERENCES

(1) Nalwa, H. S.; Miyata, S. *Nonlinear optics of organic molecules and polymers;* CRC Press: Boca Raton, FL, 1996; p 1996.

(2) Papadopoulos, M. G.; Sadlej, A. J.; Leszczynski, J. *Non-linear optical properties of matter - from molecules to condensed phases;* Springer: 2006; Vol. *1*.

(3) Verbiest, T.; Clays, K.; Rodriguez, V. *Second-order nonlinear optical characterization techniques: An introduction;* CRC Press: New York, 2009.

(4) Bishop, D. M.; Norman, P., Nonlinear optical materials. In *Handbook of advanced electronic and photonic materials and devices;* Nalwa, H. S., Ed.; Academic Press: San Diego, CA, 2001; Vol. *9*.

(5) Castet, F.; Rodriguez, V.; Pozzo, J.-L.; Ducasse, L.; Plaquet, A.; Champagne, B. Design and Characterization of Molecular Nonlinear Optical Switches. *Acc. Chem. Res.* **2013**, *46* (11), 2656−2665.

(6) Johnson, L. E.; Dalton, L. R.; Robinson, B. H. Optimizing Calculations of Electronic Excitations and Relative Hyperpolarizabilities of Electrooptic Chromophores. *Acc. Chem. Res.* **2014**, *47* (11), 3258−3265.

(7) Champagne, B.; Kirtman, B., Nonlinear optical materials. In *Handbook of advanced electronic and photonic materials and devices;* Nalwa, H. S., Ed.; Academic Press: San Diego, CA, 2001; Vol. *9*, p 63.

(8) Chopra, P.; Carlacci, L.; King, H. F.; Prasad, P. N. Ab initio calculations of polarizabilities and second hyperpolarizabilities in organic molecules with extended π-electron conjugation. *J. Phys. Chem.* **1989**, *93* (20), 7120−7130.

(9) Nakano, M.; Yamaguchi, K.; Fueno, T. Coupled-Hartree-Fock calculations of the third-order hyperpolarizabilities of substituted polydiacetylenes. *Chem. Phys. Lett.* **1991**, *185* (5), 550−554.

(10) Champagne, B.; Perpète, E.; André, J.-M.; Kirtman, B. Static vibrational polarizability of all-trans polyethylene and polysilane. *J. Chem. Soc., Faraday Trans.* **1995**, *91* (11), 1641−1646.

(11) Nakano, M.; Yamada, S.; Shigemoto, I.; Yamaguchi, K. Dynamic (hyper)polarizability density analysis based on virtual excitation processes: visualization of the dynamic electron fluctuatability of systems under time-dependent external electric fields. *Chem. Phys. Lett.* **1996**, *250* (2), 247−254.

(12) Yamada, S.; Nakano, M.; Shigemoto, I.; Yamaguchi, K. Static second hyperpolarizabilities γ of nitroxide radical and formaldehyde: Evaluation of spatial contributions to γ by a hyperpolarizability density analysis. *Chem. Phys. Lett.* **1996**, *254* (3−4), 158−164.

(13) Nakano, M.; Fujita, H.; Takahata, M.; Yamaguchi, K. Theoretical Study on Second Hyperpolarizabilities of Phenylacetylene Dendrimer: Toward an Understanding of Structure−Property Relation in NLO Responses of Fractal Antenna Dendrimers. *J. Am. Chem. Soc.* **2002**, *124* (32), 9648−9655.

(14) Zeng, Q.; Liu, L.; Zhu, W.; Yang, M. Local and nonlocal contributions to molecular first-order hyperpolarizability: A Hirshfeld partitioning analysis. *J. Chem. Phys.* **2012**, *136* (22), 224304.

(15) Seidler, T.; Krawczuk, A.; Champagne, B.; Stadnicka, K. QTAIM-Based Scheme for Describing the Linear and Nonlinear Optical Susceptibilities of Molecular Crystals Composed of Molecules With Complex Shapes. *J. Phys. Chem. C* **2016**, *120* (8), 4481−4494.

(16) Nakano, M.; Fukui, H.; Minami, T.; Yoneda, K.; Shigeta, Y.; Kishi, R.; Champagne, B.; Botek, E.; Kubo, T.; Ohta, K.; Kamada, K. (Hyper)polarizability density analysis for open-shell molecular systems based on natural orbitals and occupation numbers. *Theor. Chem. Acc.* **2011**, *130* (4−6), 711−724.

(17) Yamaguchi, K. The electronic structures of biradicals in the unrestricted Hartree-Fock approximation. *Chem. Phys. Lett.* **1975**, *33* (2), 330−335.

(18) Malrieu, J.-P.; Trinquier, G. A Recipe for Geometry Optimization of Diradicalar Singlet States from Broken-Symmetry Calculations. *J. Phys. Chem. A* **2012**, *116* (31), 8226−8237.

(19) Yamanaka, S.; Okumura, M.; Nakano, M.; Yamaguchi, K. EHF theory of chemical reactions Part 4. UNO CASSCF, UNO CASPT2 and R(U)HF coupled-cluster (CC) wavefunctions. *J. Mol. Struct.* **1994**, *310*, 205−218.

(20) Kitagawa, Y.; Saito, T.; Nakanishi, Y.; Kataoka, Y.; Matsui, T.; Kawakami, T.; Okumura, M.; Yamaguchi, K. Spin Contamination Error in Optimized Geometry of Singlet Carbene (1A1) by Broken-Symmetry Method. *J. Phys. Chem. A* **2009**, *113* (52), 15041−15046.

(21) de Wergifosse, M.; Liégeois, V.; Champagne, B. Evaluation of the molecular static and dynamic first hyperpolarizabilities. *Int. J. Quantum Chem.* **2014**, *114* (14), 900−910.

(22) de Wergifosse, M.; Champagne, B.; Ito, S.; Fukuda, K.; Nakano, M. Challenging compounds for calculating molecular second hyperpolarizabilities: the triplet state of the trimethylenemethane diradical and two derivatives. *Phys. Chem. Chem. Phys.* **2016**, *18* (9), 6420−6429.

(23) de Wergifosse, M.; Wautelet, F.; Champagne, B.; Kishi, R.; Fukuda, K.; Matsui, H.; Nakano, M. Challenging Compounds for Calculating Hyperpolarizabilities: p-Quinodimethane Derivatives. *J. Phys. Chem. A* **2013**, *117* (22), 4709−15.

(24) Nakano, M.; Kishi, R.; Nitta, T.; Kubo, T.; Nakasuji, K.; Kamada, K.; Ohta, K.; Champagne, B.; Botek, E.; Yamaguchi, K. Second hyperpolarizability (γ) of singlet diradical system: dependence of gamma on the diradical character. *J. Phys. Chem. A* **2005**, *109* (5), 885−91.

(25) Nakano, M.; Minami, T.; Fukui, H.; Yoneda, K.; Shigeta, Y.; Kishi, R.; Champagne, B.; Botek, E. Approximate spin-projected spin-unrestricted density functional theory method: Application to the diradical character dependences of the (hyper)polarizabilities in p-quinodimethane models. *Chem. Phys. Lett.* **2010**, *501* (1−3), 140−145.

(26) Yamada, S.; Nakano, M.; Nagao, H.; Yamaguchi, K. Electron correlation and structure dependencies of the second hyperpolarizability of ethylene. *Int. J. Quantum Chem.* **1999**, *71* (2), 177−183.

(27) Mondal, A.; Hatua, K.; Nandi, P. K. Static second hyperpolarizability of twisted ethylene: A comprehensive computational study. *J. Theor. Comput. Chem.* **2015**, *14* (08), 1550060.

(28) Frisch, M. J.; Trucks, G. W.; Schlegel, H. B.; Scuseria, G. E.; Robb, M. A.; Cheeseman, J. R.; Scalmani, G.; Barone, V.; Mennucci, B.; Petersson, G. A.; et al. *Gaussian 09;* Gaussian, Inc: Wallingford, CT, 2009.

(29) Bonness, S.; Fukui, H.; Yoneda, K.; Kishi, R.; Champagne, B.; Botek, E.; Nakano, M. Theoretical investigation on the second hyperpolarizabilities of open-shell singlet systems by spin-unrestricted density functional theory with long-range correction: Range separating parameter dependence. *Chem. Phys. Lett.* **2010**, *493* (1−3), 195−199.

DOI: 10.1021/acs.jpca.6b02076
J. Phys. Chem. A 2016, 120, 2727−2736